ACS Catalysis

Review

pubs.acs.org/acscatalysis

Recent Development of Molybdenum Sulfides as Advanced Electrocatalysts for Hydrogen Evolution Reaction

Ya Yan,[†] BaoYu Xia,[†] Zhichuan Xu,[‡] and Xin Wang*[,†]

[†]School of Chemical and Biomedical Engineering, Nanyang Technological University, 62 Nanyang Drive, Singapore 637459, Singapore

[‡]School of Materials Science and Engineering, Nanyang Technological University, 50 Nanyang Avenue, Singapore 639798, Singapore

ABSTRACT: Hydrogen is expected to play a major role in the development of sustainable energy and environment. Electrocatalytic hydrogen evolution reaction (HER) is known as an efficient method for large-scale hydrogen production, and in this electrochemical process, efficient and low-cost electrocatalysts are indispensable. Recent advances have revealed that nanostructured molybdenum sulfides (MoS*x*) would be promising alternatives to Pt for the electrochemical generation of hydrogen from water. In this review, we focus on the recent progress on MoS*x*-based materials as electrocatalysts toward the HER under acidic condition. Moreover, future research scope and important challenges emerging from MoS*x* nanostructures are discussed toward the development of more advanced and efficient electrocatalysts for HER.

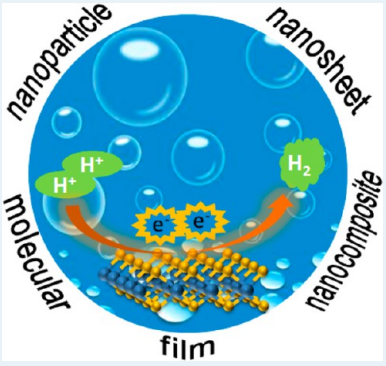

KEYWORDS: *molybdenum sulfides, electrocatalysts, nanostructures, hydrogen evolution reaction, activity, stability*

INTRODUCTION

The development of modern society has created a huge demand for renewable and environmentally friendly energy sources.[1] Hydrogen (H_2), as an ideal energy carrier, is proposed to be a major energy resource for the future world. Today, hydrogen is mainly produced from natural gas via steam methane reforming (i.e., the reaction of methane and water to form hydrogen and carbon dioxide).[2,3] Therefore, hydrogen manufacturing currently has a large greenhouse-gas footprint, which is neither renewable nor carbon-neutral. Compared with the widely employed steam-reformed hydrogen, electrocatalytic production of hydrogen from water splitting can be renewable and environmentally friendly.

The water splitting reaction can be divided into two half-reactions: the oxygen evolution reaction (OER) and hydrogen evolution reaction (HER). The HER is the reductive half-reaction of water splitting ($2H^+ + 2e^- \rightarrow H_2$), which needs a catalyst to reduce the overpotential and consequently increase the efficiency of this important electrochemical process.[4,5] Compared with alkaline electrolytes, acidic electrolytes are more favorable because these units are more compact and could potentially run in reverse mode to produce electricity (i.e., in fuel cells).[6] Currently, the most effective catalyst for the HER under acidic condition is well-known to be Pt, which has near-zero overpotential.[6] But the high price and shortage of Pt reserve prohibits its commercial application for the HER. Therefore, it remains challenging to develop highly effective alternative HER electrocatalysts with high abundance and low cost.

The study on electrochemical hydrogen evolution on molybdenum sulfides can be traced back to 1970s,[7] but the progress has been very slow because of the poor activity for bulk MoS_2.[8] Recent advances in material science and nanotechnologies have revealed that transition metal chalcogenides,[9,10] especially nanostructured MoS*x*, ($x \approx 2$ to 3),[9,10] would be promising and inexpensive alternatives to Pt for the electrochemical generation of hydrogen from water.[11−14] By analyzing the similarity between the metallic MoS_2 and the natural HER enzymatic catalysts, such as hydrogenases and nitrogenases that possess active centers consisting of Fe, Ni, and Mo, Hinnemann et al. reported that the under-coordinated sulfur atoms at the edges of MoS_2 have very similar properties to those of the active enzymatic centers,[15] and this was further verified experimentally for the nanoparticles of MoS_2 were shown to be active catalyst for HER.[16] Since then, MoS*x*-based nanocatalysts have been extensively investigated for the HER. Nanostructured MoS*x* can provide a much higher specific surface area and more active sites as compared with its bulk counterpart. This is beneficial to the HER process because the reactant diffusion, charge transfer, and even the interaction between the catalytic materials and the reaction systems could be significantly enhanced.[17] MoS*x* nanomaterials can be obtained by several methods, including mechanical or chemical exfoliation, chemical vapor deposition (CVD), and hydrothermal/solvothermal methods with different starting reagents, leading to materials with tunable stoichiometry, structure, and morphology.[18,19] Apart from designing MoS*x* at the nanoscale, optimized and enhanced properties can also be achieved by the

Received: January 17, 2014
Revised: March 20, 2014
Published: April 17, 2014

 © 2014 American Chemical Society

modification of the host material (e.g., with Co and carbon materials and so on).[20−22]

Considering the rapid progress and new achievements of MoS*x* materials as catalysts for sustainable hydrogen evolution, a detailed and critical review is highly necessary to fully cover this thriving field and motivate further scientific activities. To the best of our knowledge, only a few perspective papers were published relating to the HER process.[11,12,23,24] In this review, we focus on the recent development of MoS*x*-based nanostructures as HER electrocatalysts in acid media. First, we introduce the electrochemical evaluation basics for the HER process based on the structure and properties of MoS*x*. Consequently, we summarize and discuss recent reports of the synthesis and hydrogen-evolving catalytic properties of MoS*x* materials. Herein we emphasize the morphology and structure control and its relationship with the catalytic activities of MoS*x* toward electrocatalytic H_2 production. Specially, we also discuss several reported molecular MoS_2 edge-site mimics on the HER performance, which were shown to be the catalytically active sites in MoS_2 nanoparticles. Finally, a brief discussion on future research direction and challenges emerging from the MoS_2 nanomaterials is described.

ELECTROCHEMISTRY AND EVALUATION OF HER

As the half-reaction for water splitting, the HER process can be explained by three possible reaction steps on various electrocatalysts in acidic media.[4,7] The first Volmer step is electrochemical hydrogen adsorption: $H_3O^+ + e^- + M \rightarrow MH_{ads} + H_2O$ (1); this is followed either by Heyrovsky step (electrochemical desorption) $MH_{ads} + e^- + H^+ \rightarrow M + H_2$ (2) or Tafel step (chemical desorption) $2MH_{ads} \rightarrow 2\,M + H_2$ (3), where M donates an empty metal active site and MH_{ads} represents an adsorbed H intermediate.[25] The HER activities of various catalysts can be summarized in the "volcano plot", as shown in Figure 1,[16] where the exchange current density for different catalysts in acids are plotted as a function of the Gibbs free energy of absorbed atomic hydrogen on catalysts.[26] An optimal HER catalyst should provide catalytic surfaces that exhibit a Gibbs free energy of adsorbed hydrogen close to zero (e.g., $\Delta G^0_H \approx 0$). Thus, the promising catalyst lies at the top of the curve (Figure 1), which is neither binding the intermediate MH_{ads} too weakly nor too strongly.[15] Accordingly, one can also easily understand why Pt is a commonly chosen catalyst for the HER. Importantly, by comparison of the exchange current densities of the common metals at their corresponding free energy of absorbed H, ΔG^0_H, the value for MoS_2 just lies below those of the noble Pt group metals, suggesting the great potential of MoS_2-based materials as an alternative to Pt for the HER.[16]

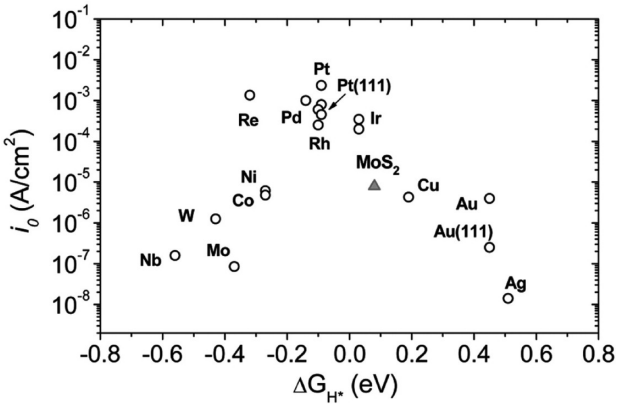

Figure 1. Volcano plot of the exchange current density as a function of the DFT-calculated Gibbs free energy of adsorbed atomic hydrogen for nanoparticulate MoS_2 and pure metals. As seen, MoS_2 follows the same trend as the pure metals. Figure reproduced with permission from ref 16. Copyright 2007 American Association for the Advancement of Science.

In electrochemical kinetics, the reaction rate of the HER, or the current density, depends on overpotential, and the relationship is known as the Butler−Volmer equation, which is given by

$$j = j_0[e^{(1-\alpha)\eta f} - e^{-\alpha\eta f}]$$

Where j is the current density, j_0 is the exchange current density, η is the overpotential, α is known as transfer coefficient and $f = F/RT$ (F is the Faraday constant, R is the gas constant, and T is the temperature in Kelvin). The value of overpotential is specific to each cell design and will vary between cells and operational conditions even for the same reaction. It often lies in the range of 0.1−0.5 V for the HER.[11] Overpotential at a specified apparent current density is a useful experimental parameter to characterize a given electrode in the working condition,[4] whereas the onset overpotential, often namely as onset potential, refers to the smallest potential where the catalyst starts to catalytically function or the HER process begins.[11] Specifically, at high overpotential ($\eta > 0.05$ V), the Butler−Volmer equation can be simplified to the form known as the Tafel equation

$$\eta = a + b\log j$$

The electrochemical evaluation for the HER at various catalytic materials are usually represented by the kinetic values of the constants a and b of the Tafel equation.[27] The constant b, defined as Tafel slope, an inherent property of the catalysts, is related to the reaction mechanism of a catalyst and is determined by the rate-limiting step of the HER. The value depends on several factors, including the reaction pathway and the adsorption conditions of the active site.[27] Because of a very high H_{ads} coverage ($\theta_H \approx 1$), the HER on a Pt surface is known to proceed via the Volmer−Tafel mechanism (eqs 1 and 3), and the Tafel step is the rate-limiting step at low overpotential, as attested by the measured Tafel slope of 30 mV dec^{-1}.[27] In the case of MoS*x*, the Tafel slope may vary significantly for different structures and properties of MoS*x* materials. Previous studies on MoS*x* catalysts have shown a large spread of Tafel slopes ranging from 40 mV to 120 mV dec^{-1}.[16,28−32]

Another evaluation of intrinsic electrocatalytic activities for electrocatalysts has often been made on the basis of relative values of log j_0 for the HER, which is an important kinetic parameter representing the electrochemical reaction rate at equilibrium. It may be understood as an indicator of the electron transfer rate of a catalyst and its magnitude determines how rapidly the electrochemical reaction can occur. Because MoS_2 is an intrinsic semiconductor with a marked anisotropic behavior in conductivity,[33,34] slow electron transport is likely the origin of the lower exchange current densities in certain molybdenum sulfide catalysts. Thus, optimizing the conductivity of those MoS*x*-based materials is a very promising pathway for developing an efficient HER electrocatalyst.[35] Details for this aspect will be discussed in later sections. Here, one important issue needs to be clarified: the comparisons

dx.doi.org/10.1021/cs500070x | ACS Catal. 2014, 4, 1693−1705

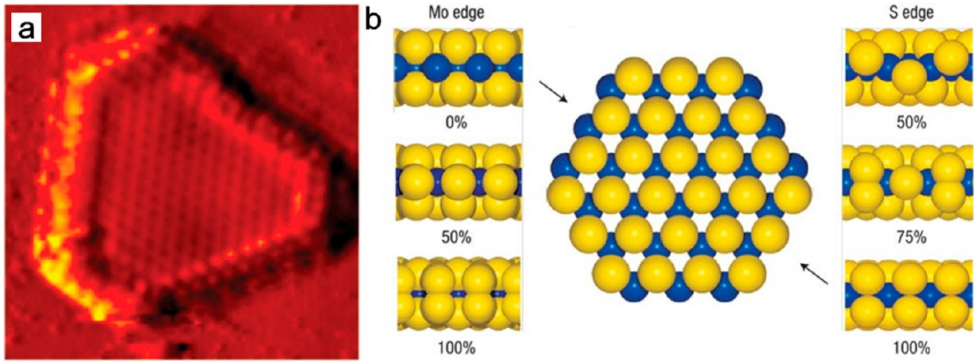

Figure 2. (a) STM on MoS_2 nanoplatelets on Au (111). (b) Molecular model of a platelet exposing both Mo and S-edges from top and side view. Mo atoms are blue, S atoms are yellow. Figures reproduced with permission from (a) ref 16, Copyright 2007 American Association for the Advancement of Science; (b) ref 34, Copyright 2007 Nature Publishing Group.

based on log j_0 values alone give only a measure of kinetics at the equilibrium or zero-polarization condition, whereas the comparisons on the basis of b values provide a complementary mechanistic aspect of the kinetic behavior under the practical operating conditions.[36] An optimal and ideal catalyst is the material that has the highest exchange current density and lowest Tafel slope. These matters are of importance to optimize the operation and performance of electrolyzers for H_2 production and especially for the selection of cathodic materials for the HER.

Besides, the intrinsic per-site activity of a catalyst is also an important metric necessary to assess the ceiling for further improvement and to guide catalyst development, which is often measured by the turnover frequency (TOF) for each active site, representing a chemical reaction rate. The value is closely related to the activity of each catalytic site of the catalysts. The difficulty in measuring a TOF is not only in determining the rate but also in counting active sites. Besides, sites may not be all identical even for the same catalyst. Practically, for different MoSx-based catalysts, the comparison of the TOFs is only meaningful when the value is taken at the same overpotential. Thus, the comparison of TOF value at zero overpotential might be more reliable because this could be deduced from the j_0.[37] In general, TOFs of transition metals range over 10 orders of magnitude (e.g., Hg has a TOF as low as ~10^{-9} s^{-1}).[25] In this review, we will evaluate the HER catalytic activity for different MoSx catalysts on the basis of the onset potential, Tafel slope, exchange current density, as well as the TOF.

■ MoS_2 STRUCTURE AND PROPERTIES

As one typical chemical composition of bulk molybdenum sulfides, MoS_2 naturally occurs as a lamellar hexagonally structure similar to graphite in which the individual S−Mo−S layers weakly interact with each other by van der Waals forces, and each layer has a thickness of ~0.7 nm.[38,39] Typically, MoS_2 occurs in two modifications, 2H and 3R. The hexagonal 2H-polytype has two layers per unit cell along the c-axis, and the rhombohedral 3R-polytype has three layers per unit cell. In nature, the 2H-type is dominant and more stable, and 3R will transform to 2H upon heating. Although for those MoS_2 nanosheets produced from chemical Li-intercalation and exfoliation, the pure 2H phase will experience phase transformation to a metastable metallic 1T phase, which causes MoS_2 evolving from the semiconducting to metallic polymorphs.[7,40,41] The conversion of 2H MoS_2 to 1T phase has been shown to be positive for its HER catalytic performance, and this will be described in more detail in the part of the section MoSx Nanosheets.

Different from the hexagonally structure of its bulk form, the MoS_2 nanocrystals often exhibit a triangular morphology and are often reported as slightly truncated triangles.[42,43] Figure 2a shows a typical scanning tunneling microscopy (STM) image of MoS_2 single sheet grown on Au(111).[16] Only one edge type is energetically favored and presented due to the triangular shape.[34] The edges of the nanoplatelets are bright rims as seen from the STM images in Figure 2a, suggesting the conductivity at the edge. DFT calculations indicate that the free energy of adsorbed H (ΔG_H) on crystalline MoS_2 (10−10) edge sites with 50% S adsorption is close to those on a hydrogenase model and Pt (close to zero) (Figure 2b). It is found that for all types of the MoS_2 edges, the electronic structure is dominated by metallic one-dimensional edge states, proving that fully sulfided Mo edges play an important role in the catalysis.[15,44]

Studies on MoS_2 nanocrystals demonstrated that the ratio of basal plane sites to edge sites could be changed with the particle size without changing the nature of the edge; this is important for us to design efficient MoS_2 catalysts.[16] After the heat treatment at different annealing temperatures (400 and 550 °C), the particle size changes, resulting in the predominance of the sulfided Mo-edge.[16] The morphology between the triangular and hexagonal form could also be changed by varying sulfiding and reaction conditions.[43] Moreover, the incorporation of cobalt (Co) or nickel (Ni) into MoS_2 can tune the intrinsic catalytic activity,[32,45] as the promoter atoms prefer to be located exclusively at the S edges. The presence of unsaturated sulfur atoms in these materials can engage in the discharge reaction and form S−H bonds and thus eventually lead to hydrogen formation.

From the above analysis, three ways can be used to improve the activity of MoSx-based electrocatalysts in this context: (1) increasing the number of the active sites per unit volume by tailoring progressively smaller nanostructures or engineering the surface structure at the atom scale or using discrete molecular units to make efficient molecular catalysts; (2) improving the conductivity and diffusion properties of MoS_2 materials by decreasing the restacking of the materials, as well as stacking the layered structure to the conductive surface to improve the electron transfer among the catalysts; and (3) enhancing the inherent activity of MoS_2 by appropriately tuning the electronic structure of the edge to improve the bond strength of the adsorbed H. Along these approaches, various

dx.doi.org/10.1021/cs500070x | ACS Catal. 2014, 4, 1693−1705

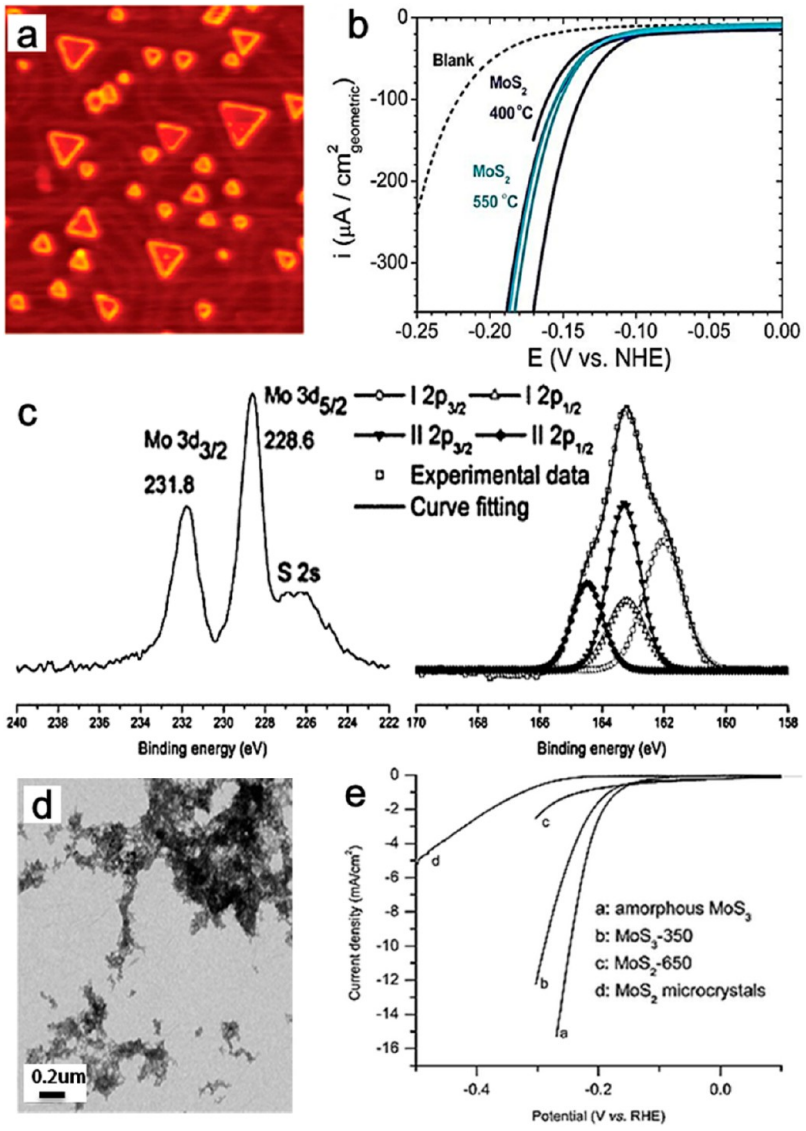

Figure 3. (a) STM image of MoS_2 nanoparticles on Au (111), from a sample annealed to 550 °C, (470 Å by 470 Å, 1.2 nA, 1.9 V). (b) Polarization curves for the HER on different MoS_2 samples, as well as a blank sample. (c) XPS spectra of the MoS_3 particles: (left) Mo 3d and S 2s region; (right) S 2p region. (d) TEM image of the MoS3 particles. (e) Polarization curves of carbon paste electrodes modified with a layer of MoS*x* species. The measurements were conducted at 1.0 M H_2SO_4; scan rate: 5 mV s^{-1}. Figures reproduced with permission from (a,b) ref 16, Copyright 2007 American Association for the Advancement of Science; (c–e) ref 48, Copyright 2012 Royal Society of Chemistry.

MoS*x*-based nanostructures have been developed as electrocatalysts for the HER, and the details will be elaborated below.

MOS*X*-BASED ELECTROCATALYSTS FOR HER

MoS*x* Nanoparticles. Since the first DFT prediction in 2005 that the metallic edges of MoS_2 nanocrystals were electrocatalytically active for hydrogen evolution [15] Jaramillo and co-workers experimentally verified the HER activity of MoS_2 nanoparticles two years later.[16] MoS_2 samples on a clean Au (111) substrate were prepared by physical vapor deposition of Mo in a background of H_2S, followed by annealing the samples at 400 or 550 °C (Figure 3a). The obtained MoS_2 on Au (111) showed overpotentials at about −0.15 V, Tafel slopes of 55–60 mV dec^{-1}, and exchange current densities in the range of 1.3×10^{-7} to 3.1×10^{-7} A cm^{-2} for all MoS_2 samples (Figure 3b,c). Furthermore, for the direct site-to-site comparison, the TOF of the MoS_2 edge were determined and found to be 0.02 s^{-1} (at 0 mV vs RHE (reversible hydrogen electrode)), which was rather high even for metal and was not much lower than that of Pt (TOF = 0.9 s^{-1}).[16] Following this work, Bonde et al. prepared carbon paper loaded MoS_2 nanoparticles and showed an onset potential of about −0.2 V vs RHE and a Tafel slope of 120 mV dec^{-1}.[32] Compared to the Tafel slope to that of Au (111)-supported MoS_2 nanoparticles, this much higher Tafel slope was attributed to the transport limitations through the fibrous, porous network of Toray carbon paper.

Combining DFT calculation and electrochemical measurements, it was further found that the activity of MoS_2 nanoparticles could be significantly increased by doping with Co.[32] The incorporation of Co into the S-edges is able to reduce the binding energy of hydrogen from 0.18 to 0.10 eV, comparable to 0.08 eV for the Mo-edge. It is known that the binding free energy ΔG_H can affect the hydrogen coverage, and a smaller absolute value of ΔG_H (close to zero) will result in a higher activity. Thus, it is expected that the decreased ΔG_H for

dx.doi.org/10.1021/cs500070x | ACS Catal. 2014, 4, 1693–1705

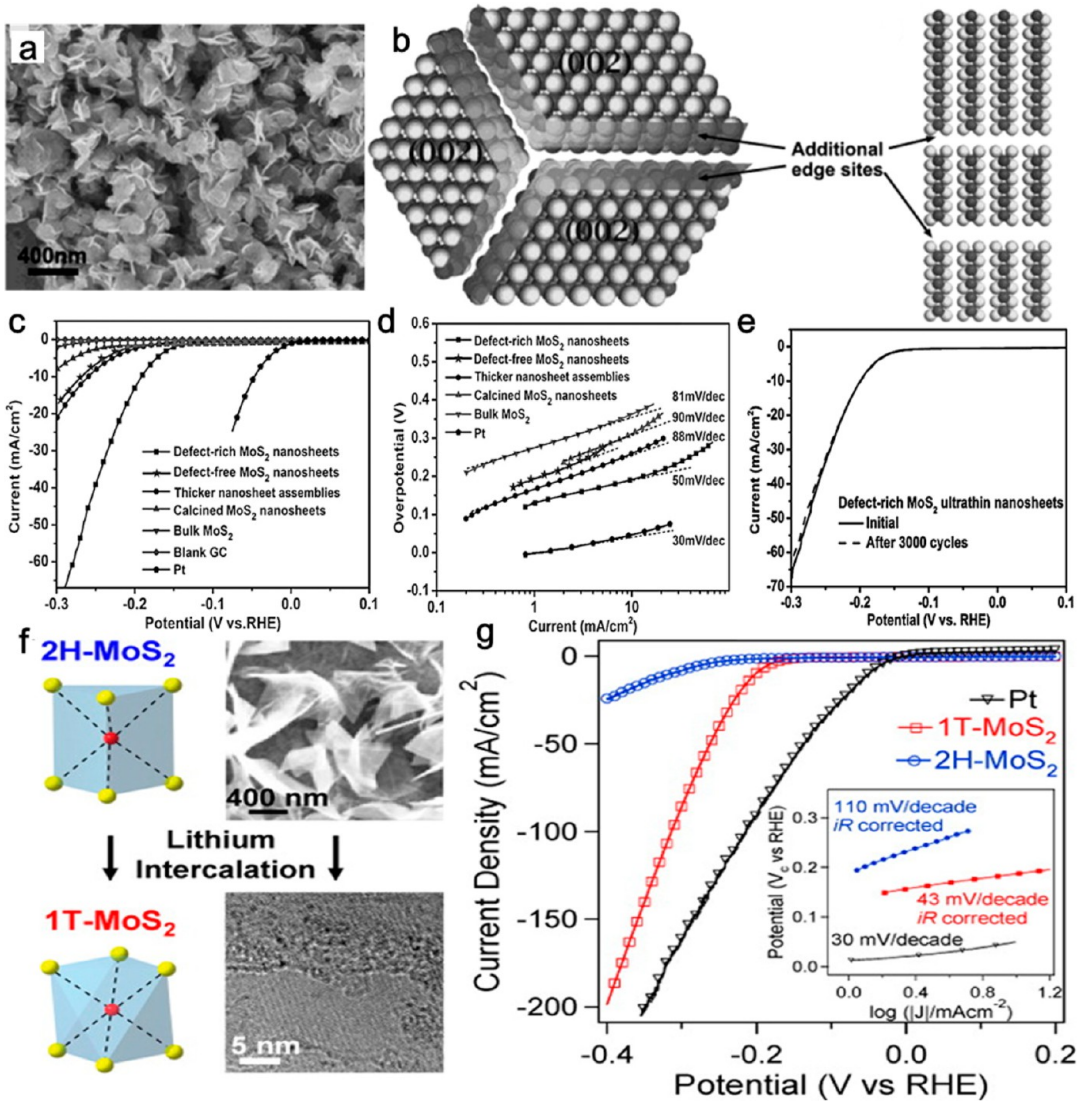

Figure 4. (a) TEM images of the defect-rich MoS_2 ultrathin nanosheets. (b) Atomic reconstruction of (a). Additional active edge sites are designated by gray shading. (c) Polarization curves of various samples as indicated and (d) corresponding Tafel plots. (e) Durability test showing negligible current loss even after 3000 CV cycles. (f) 2H and 1T models for MoS_2 and corresponding top-down SEM image of as-grown 2H-MoS_2 and unstable HRTEM image of chemically exfoliated 1T-MoS_2 nanosheets and (g) corresponding polarization curves. Figures reproduced with permission from (a–e) ref 59, Copyright 2013 Wiley; (f, g) ref 66, Copyright 2013 American Chemical Society.

the S-edge may increase the H coverage, which in turn increases the interaction between two neighboring H* species and decreases the binding free energy for subsequent hydrogen atoms.[11] This study provides a promising way to improve the inherent activity of MoS_2 activity by doping heteroatoms and optimizing the binding energy of hydrogen. However, it is noted that the MoS_2 nanocrystals prepared by the high-temperature sulfiding procedure is energy intensive and requires a large investment in equipment, which hampers its large-scale application.

In addition, considering that heat treatment may decrease the number of edge sites, which is directly proportional to the reaction rate, an important issue that should be addressed for all kinds of the MoS*x*-based catalysts is the underling influence of heat treatment on their catalytic activity for the HER. Jaramillo and co-workers found the exchange current densities (per MoS_2 coverage) of the samples sintered at 550 °C were significantly lower than those prepared at 400 °C because of the decreased edge length per area of MoS_2.[16] Similar results were also reported in the study of other kinds of MoS*x* catalysts.[46−48] After annealing at high temperature, the particle size increases and the degree of crystallinity is improved. The final lower HER activity was explained by the decrease of the amount of unsaturated sulfur atoms on the surface of these sulfide materials (Figure 3f).[48] In the case of the MoS_2 sample with vertically aligned layers, STEM images showed that, after annealing, they converted into particulate morphology with randomly oriented platelet-like nanoparticle with a dimension of tens of nanometers, indicating that driven by the tendency to decrease the overall surface energy, the growth of these nanoparticles reduced the number of edge sites.[47]

The edges of MoS_2 are identified as the active sites for the HER, where the unsaturated S atoms are exposed and can absorb H with a small free energy. Amorphous MoS*x* has many defect sites and coordinately unsaturated S atoms, which makes it a potentially better HER catalyst. Vrubel and co-workers described a simple chemical method to prepare amorphous MoS_3 particles by acidification of a solution of MoO_3 and Na_2S

dx.doi.org/10.1021/cs500070x | ACS Catal. 2014, 4, 1693−1705

(Figure 3d).[48] After loading onto FTO, the assembled electrode displayed excellent HER activities with Tafel slopes in the range of 40−45 mV dec^{-1}. It was found that the freshly obtained amorphous MoS_3 particles were reduced to another form of molybdenum sulfide consisting of catalytically active S_2^{2-} ligand during the preactivation process (Figure 3e). In parallel, by acidification of a solution of $(Mo_7O_{24}(NH_4)_6{\cdot}4H_2O$ and Na_2S, another active amorphous MoS*x* electrocatalyst was also synthesized.[49] More unsaturated S atoms were found in those amorphous MoS*x* electrocatalysts in comparison to highly crystalline MoS_2. The obtained catalysts then could be deposited onto various types of substrates. It was found that domains resembling MoS_2 in both composition and chemical state were created during the preactivation process, which might contribute a lot to the enhanced HER activity.[49] Thus, the effective pathway to achieve high HER activity for MoS*x* nanoparticles is to increase the density of active edges by introducing a small nanosized dimension together with amorphous structure as well as improving the conductivity of the whole catalyst system via support interactions.[50−52]

However, one significant concern for those amorphous MoS*x* particles is the apparent Tafel slope variance (40−60 mV dec^{-1}) with the changing of substrate and catalyst loading. To circumvent this issue, Vrubel et al. recently highlighted the benefits of transitioning from linear sweep voltammetry (LSV)-based analysis to electrochemical impedance spectroscopy-(EIS)-based analysis of Tafel slopes.[53] They demonstrated the possibility of identifying a slow electron transport process in the HER catalyzed by molybdenum sulfides. Using this analytical method, the as-prepared amorphous MoS_3/Vulcans C hybrid demonstrated a superior HER activity with a Tafel slope as low as 36 mV dec^{-1}, indicating a fast electron transport process, which is the smallest measured Tafel slope to date for a MoS*x*-based catalyst. This interesting study provides a new experimental approach for investigating the significant electronic coupling between MoS*x* catalysts and conducting carbon materials.

MoS*x* Nanosheets. In addition to MoS*x* nanoparticles, MoS_2 nanosheets have also been investigated recently for their dimensional characteristics. It is known that the resistivity through the basal planes of layered MoS_2 has been measured to be 2200 times larger as compared to the value along the individual MoS_2 nanosheets.[11] The electron transfer of MoS_2 nanoparticles has to proceed from the support to the bottom layer and then further through several platelet interfaces to reach all the edges, which greatly complicates the electron transfer process and leads to significantly increased resistance. Accordingly, it was proposed that the single-layer nanoplatelet could be a better structure compared to a multilayer nanoparticle because electrons only need to be transferred from the support to the platelets.[11] Previously, mechanical exfoliated semiconducting 2H-MoS_2 nanosheets were investigated for H_2 evolution and showed only marginally improved catalytic performance.[54,55] This is because of their tendency to restack during material processing, which will not only prevent the vertical charge transport but also limit the protons access to the catalytically active sites. Thus, decorating the nanosheets with electrically conductive metal nanoparticles, such as Au, were conducted to inhibit restacking and improve electron transfer along interplanar directions and mass transport.[56] However, the obtained gold-nanoparticle-decorated MoS_2 sheets still show limited HER performance. A recent study showed that the catalytic activity of MoS_2 for HER decreases by a factor of ∼4.47 for the addition of every one additional layer on the MoS_2 atomically thin films. This similar layer-dependent trend is also found in the MoS_2 pyramid platelets with rich edges.[57] With those in mind, designing ultrathin MoS*x* nanosheets with more exposed edges may be a good consideration.[58] Xie's group developed defect-rich MoS_2 ultrathin nanosheets (Figure 4a) and highlighted that their MoS_2 material contained abundant defects, which resulted in partial cracking of the catalytically inert basal planes, leading to the exposure of additional active edge sites (Figure 4b).[59] The obtained defect-rich MoS_2 ultrathin nanosheets exhibited an excellent HER activity with an onset potential of 0.12 V vs RHE and a Tafel slope of 50 mV dec^{-1}, as well as a prominent electrochemical durability (Figure 4c−e). Then, in order to optimize the interdomain conductivity of the defect-rich MoS_2 nanosheets, recently, they put forward the elemental incorporation by controllable disorder engineering. Thus, the balance between rich active sites and good conductivity in oxygen-incorporated MoS_2 nanosheets is realized for efficient HER performance.[60]

From another perspective, the important factor governing the amount of edges is the relative surface energy of the edges comparing to the basal plane. With the surface energy of MoS_2 edge reported to be 100 times larger than that of the basal plane,[61] lowering the edge surface energy could be another effective way to increase the amount of edges. Along this direction, a recent study shows that MoS_2 synthesized in an ionic liquid (IL) consisted of randomly packed and almost exclusively single sheets of MoS_2.[62] Following this, they demonstrated well how to control these features during the synthesis by using a range of ionic liquids as media.[63] The synthesized MoS_2 materials showed great promise as highly active HER catalysts. Importantly, this study provides new thought for a synthetic strategy to increase the number of edges on the catalyst by employing an IL with specific solvation properties.

In most experimental studies, the 2H-MoS_2 bulk crystal is used to prepare the isolated MoS_2 nanosheets. Such 2H-MoS_2 can transform into a metallic 1T phase by exfoliation with Li intercalation (Figure 4f).[64,65] By comparison with the 2H-type, the obtained 1T- MoS_2 nanosheets showed dramatically enhanced HER catalysis with an onset potential of 0.15 V vs RHE and a Tafel slope of 43 mV dec^{-1} (Figure 4g). In contrast, exfoliated MoS_2 nanosheets consisting of both 2H and 1T just showed a limited HER performance (Tafel slope of 94 mV dec^{-1}).[55] This high activity was attributed mostly to the facile electrode kinetics and low-loss in electron transport other than the proliferation of active sites in the 1T-MoS_2 nanosheets.[66] It is worth mentioning that the poor stability of the 1T- MoS_2 nanosheets for the HER was also observed, showing the slow reconversion of the metallic 1T polymorph to the semiconducting 2H phase even under moderate-temperature annealing (e.g., 95 °C).[65] Therefore, the catalytic property for the 1T phase remains an important and open question and requires further investigations.[67]

MoS*x* Film. By far, MoS*x* materials composed of nanoparticle and nanosheet structure have shown great advantages and attracted much interest for HER. MoS*x* films composed of 0D/1D or 2D structures have also been found to be a promising catalyst for the HER simultaneously.[31] Recently, a novel thin film consisting of stoichiometric MoS_2 nanoparticles was prepared by a electrodeposition method in the ionic liquids (IL) electrolyte (Figure 5a).[68] Here, ILs were employed as

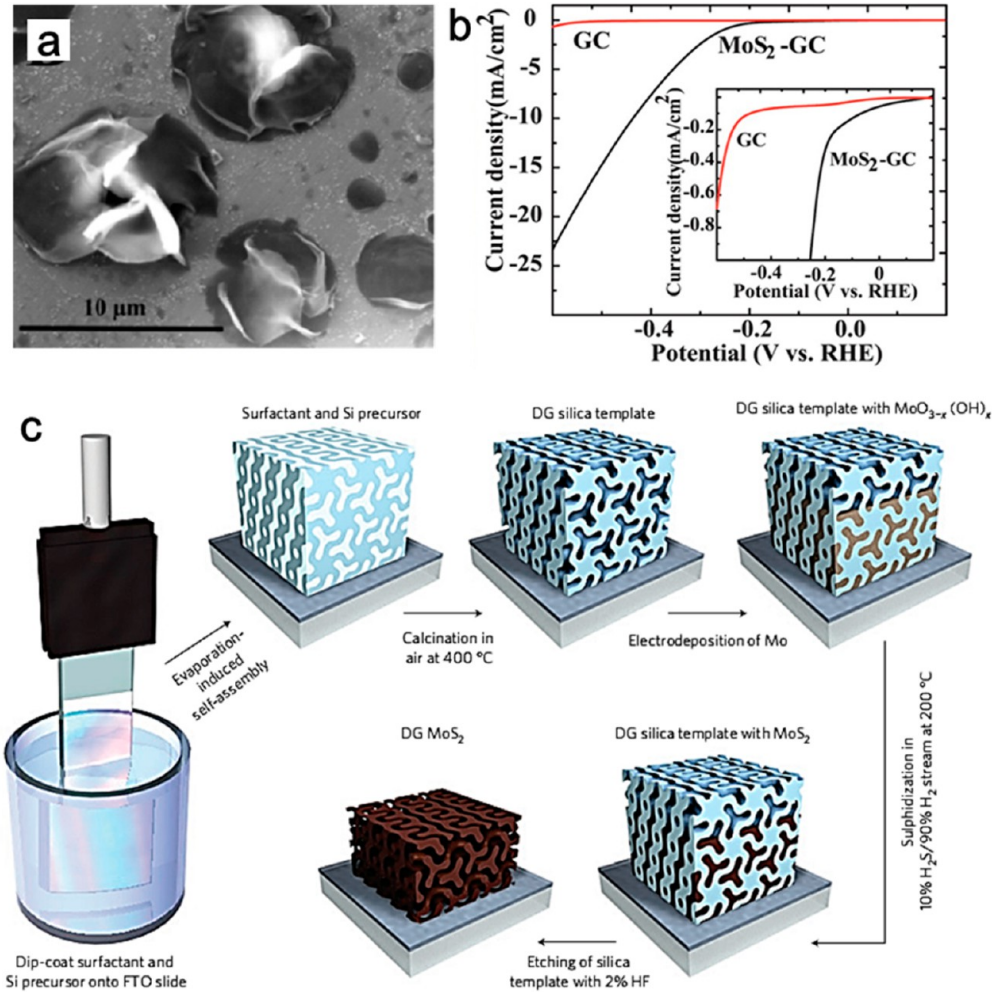

Figure 5. (a) SEM image of chronoamperometrically at −2.7 V vs Pt electrodeposited MoS_2 over glassy carbon electrodes showing the formation of flower morphology. (b) HER in 0.5 M H_2SO_4 at the scan rate of 2 mV/s at GC and at MoS_2 electrodeposited over GC, the inset showing the corresponding onset potential. (c) Synthesis procedure and structural model for mesoporous MoS_2 with double-gyroid (DG) morphology. Figures reproduced with permission from (a, b) ref 68, Copyright 2013 American Chemical Society; (c) ref 28, Copyright 2012 Macmillan Publishers Limited.

unique electrolytes for the electrochemical reduction of reactive metal Mo due to their negligible vapor pressure, wide electrochemical window, and high ionic conductivity. The obtained MoS_2 films showed flower shape morphology with active edge sites. The hydrogen evolution test with the film yielded a Tafel slope of 106 mV dec^{-1} (Figure 5b), suggesting that the rate-determining step of H_2 evolution on the MoS_2 film was a slow adsorption of protons on the catalyst surface. To increase the amount of active sites of MoS_2 film, Hu and his co-workers reported the successful fabrication of amorphous MoS*x* films via simple electropolymerization procedures. The obtained MoS*x* thin film could be a mixture of MoS_3 and MoS_2 nanoparticles. Their results revealed that the active component for the electrocatalytic HER was identified as amorphous MoS_2. Significantly, such amorphous MoS*x* film showed good compatibility in a wide pH range (e.g., 0−13) and gave a decent Tafel slope as low as 40 mV dec^{-1}. It was different from those of MoS_2 nanoparticles,[16,32] and a slow electrochemical desorption on the MoS*x* films was proposed to be the rate-limiting step. Due to the amorphous nature, the MoS*x* films may have more unsaturated active sites than that of MoS_2 single crystals and MoS_2 nanoparticles and thus lead to the better HER activity. Besides, it was worth noting that the electrodeposition method not only can easily introduce the transition metal ions into the MoS*x* electrocatalysts (this will be described in more detail in the following paragraph) but also can permit the incorporation of MoS*x* electrocatalysts within a hybrid photo−catalyst or −electrode system.[69−71] Different from the electrdeposition process, a self-assembled monodispersed molybdenum sulfide film consisting of ultrasmall amorphous MoS*x* nanoparticles (with diameters of about 1.47 nm) on Au surface was fabricated by just using ultrasonication and centrifugation steps.[72] The assembled film showed a high electrocatalytic performance with an onset potential as low as −0.09 V vs RHE and a Tafel slope of 69 mV dec^{-1} for the HER. This relatively high activity was proved to arise from highly active S edges as revealed by a low ratio of Mo to S and the possible rearrangement of the S rich nanoparticles on Au, as well as the excellent electrical coupling to the underlying Au electrode via the formation of the Au−S bond. This work effectively showed a facile way to synthesize active monodispersed molybdenum sulfide nanoparticles for the HER and a new approach to achieve enrichment of S edges by constructions of molybdenum sulfides films.

In order to further enhance the activity of the amorphous MoS*x* film, Hu's group attempted to dope the films with

dx.doi.org/10.1021/cs500070x | *ACS Catal.* 2014, 4, 1693−1705

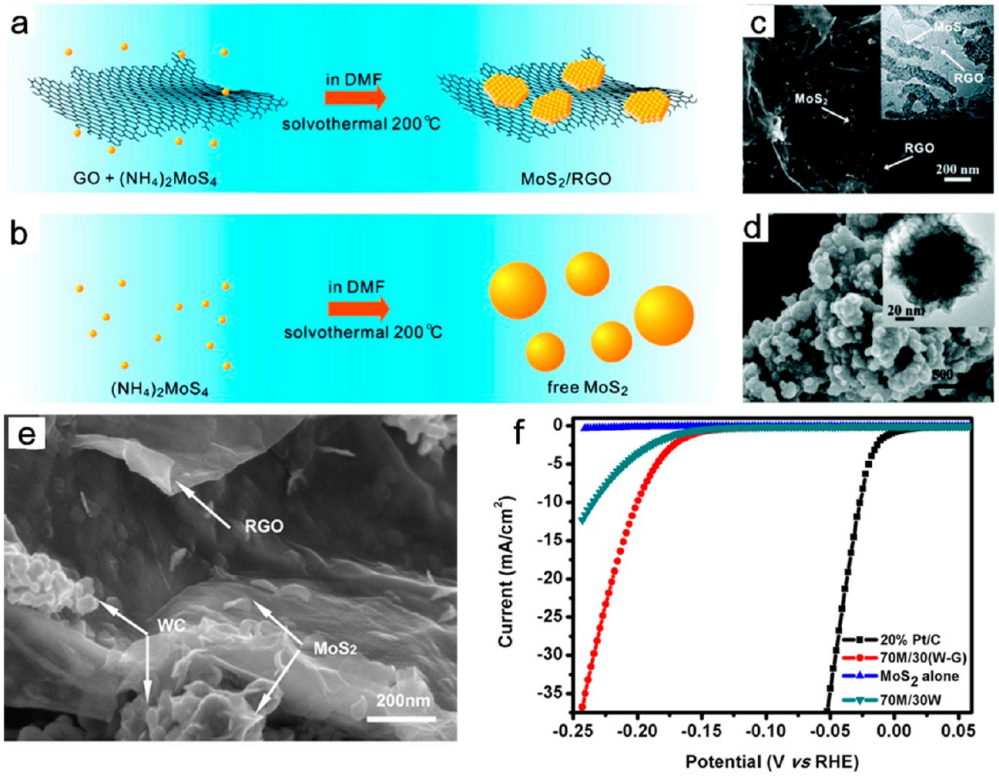

Figure 6. (a,b) Schematics of solvothermal synthesis (a) with graphene oxide sheets for MoS_2/RGO hybrid synthesis and (b) without graphene oxide sheets, resulting in large, free MoS_2 particles. (c,d) SEM and TEM (inset) images of the MoS_2/RGO hybrid (c) and of the free MoS_2 particles (d). (e) FESEM image of MoS_2/WC/RGO composites. (f) Polarization curves for the as-prepared samples. Figures reproduced with permission from (a–d) ref 29, Copyright 2011 ACS; (e,f) ref 82, Copyright 2013 Royal Society of Chemistry.

transition metal ions by cyclic voltammetry of aqueous solutions containing MCl_2 (M = Mn, Fe, Co, Ni, Cu, Zn) and $(NH_4)_2[MoS_4]$.[73] Experimental results demonstrated that the resulting Mn–, Cu–, and Zn–MoS_3 films showed a similar Tafel slope to the MoS_3 films, whereas the Fe–, Co–, and Ni–MoS_3 films were significantly more active than the Mn–, Cu–, and Zn–MoS_3 films with much higher exchange current densities (j_0). They proposed that those "'defect sites"' in the amorphous materials can be considered as unsaturated Mo and S sites where HER may take place; therefore, the presence of certain promoter ions could enhance the activity of these unsaturated sites, leading to higher intrinsic activity. It was also found that the promotion effect is significant at pH = 7 but not at pH = 0. This finding may be because the HER catalysis is dominated by the activity of the Mo sites at pH = 0, whereas the promoted S sites contribute significantly to the overall activity of catalysis at pH = 7. However, there is still no clear evidence proving the Co-doping in this material except for the XPS analysis evidenced the presence of Co, the DFT calculation of the Co-doped MoS_2 revealed some clues regarding the activity promotion for the introduction of Co doping.[32] Moreover, a potential problem for those amorphous MoS*x* catalytic materials is the poor stability. The preliminary results indicate the poor crystallinity of these sulfides may lead to relatively high solubility and poor electrochemical stability in the acid electrolyte. Further study on the long-term performance is still needed before these materials could be potentially used in large scale applications. Significantly, Barber's group recently reported a highly crystalline layered ternary sulfide copper–molybdenum-sulfide (Cu_2MoS_4) electrocatalyst,[74] which showed very good catalytic activity for HER. Moreover, this Cu_2MoS_4 catalyst was found to be stable during electrocatalytic hydrogen generation, representing an attractive alternative to platinum together with other transition-metal-containing ternary sulfides.[75]

Apart from the films consisting of MoS*x* nanoparticles, those films stemming from the MoS_2 nanosheets have also been reported. But for the layered MoS_2, it is likely that a thermodynamic driving force impedes the formation of atomically undercoordinated and highly energetic edge sites at the surface relative to nonactive basal sites due to its anisotropic nature. Thus, there is now growing interest to achieve high densities of exposed edges by engineering the structure of the layered MoS_2 at the nanoscale. For example, Jaramillo et al. successfully designed and prepared an extended 3D mesoporous MoS_2 thin film with double-gyroid morphology to preferentially expose more edge sites (Figure 5c).[28] It was proposed that a large fraction of exposed edge sites arose from the high surface curvature, which, along with its high surface area, leads to the excellent HER activity. The measured Tafel slope for this mesoporous MoS_2 film was about 50 mV dec^{-1}. It was expected that this activity could be further potentially improved by incorporating into a large conductive support with macrostructure to minimize charge transport limitations and into a assembled membrane electrode to minimize mass transport limitations or by adding dopants to decrease the resistivity of the MoS_2 film.[76] Simultaneously, Cui's group fabricated a MoS_2 thin film with vertically aligned layers by a sulfurization process, thereby maximally exposing the edges on the surface.[47] The obtained edge-terminated MoS_2 film yielded an exchange current density as high as 2.2×10^{-6} A/cm^2, which is about ten times higher than previous

dx.doi.org/10.1021/cs500070x | ACS Catal. 2014, 4, 1693–1705

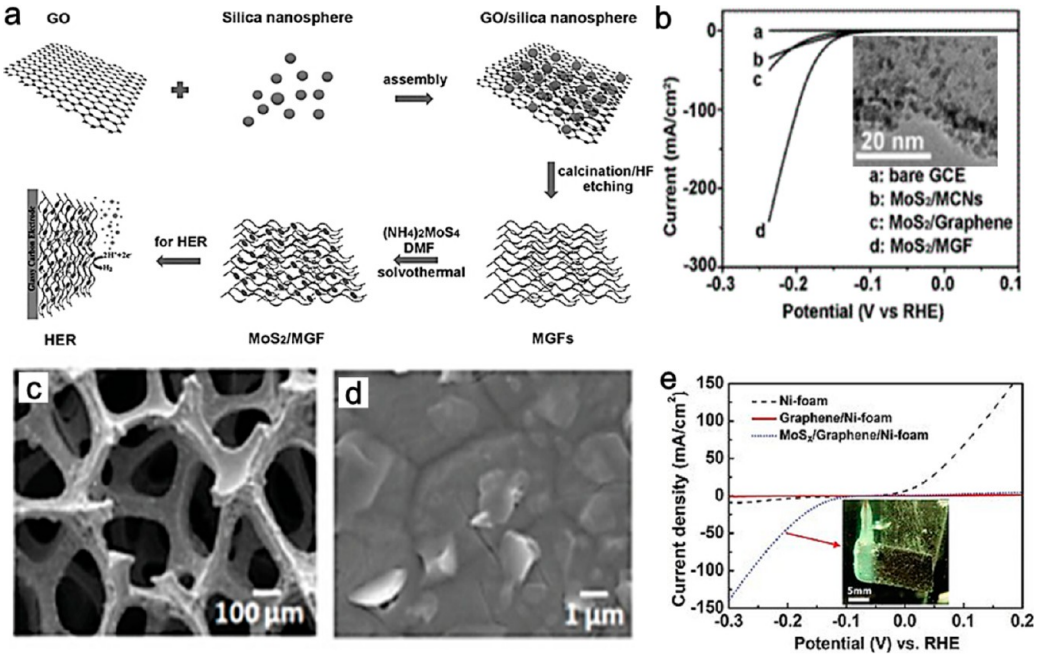

Figure 7. (a) Illustration of the synthesis procedures of MoS_2/MGF used as an electrocatalyst for hydrogen evolution reaction. (b) LSV polarization curves for various samples in 0.5 m H_2SO_4 with a hybrid catalyst loading of 0.21 mg cm^{-2}. Scan rate: 2 mV s^{-1}. The inset of (b) is the TEM image of MoS_2/MGF. (c) SEM image of graphene-protected Ni foam on which MoS_2 catalysts were grown. (d) SEM image of the magnified region in the central image of (c). (e) The measurements were performed in a 0.5 M H_2SO_4 solution. The inset of (f) is a photograph of Ni foam coated with graphene and MoS_2. Figures reproduced with permission from (a,b) ref 85, Copyright 2013 Wiley; (c–e) ref 46, Copyright 2012 Wiley.

MoS_2 nanoparticle-based electrodes.[16] A TOF of 0.013 s^{-1} at 0 V vs RHE was also measured, which was very close to the reported value (0.016 s^{-1}) for the MoS_2 nanoplatelet catalysts, thus confirming that nearly all of the surface sites on edge-terminated films are catalytically active.[16] Further improvement of this film on the HER performance could be achieved by tuning the substrate morphology or the choice of different substrate.[77]

MoS*x* Composites. Although great advances have been achieved in MoS*x* electrocatalysts based on nanoparticle, nanosheets, and film structures for the HER, it is noted that the extremely low conductivity is still an inherent problem of using single MoS*x* materials as catalysts for the electrochemical HER. Moreover, aggregation of MoS*x* materials also affects the dispersion and results in the decrease of activity. Thus, the modification of MoS*x* materials with conductive templates or supports is proposed to be an effective way to improve the catalytic activity of the host material. By now, quite a few investigations have proved that the HER performance of MoS*x* could be significantly enhanced by incorporating MoS_2 with graphene, carbon nanotube (CNTs), and other mesoporous carbon to form MoS*x*-based hybrid or composite.[78−81] The nanocarbons serve as templates for mediating the growth of the MoS*x* and formation of specific structures, which improves the dispersion of MoS*x* materials and enhances the conductivity of whole MoS*x* composites.

Inspired by the high surface area and good conductivity, especially the similar two-dimension (2D) structural properties, reduced graphene oxide (RGO) sheets were introduced to form MoS_2/RGO hybrid (Figure 6a,b).[29] The resultant composite demonstrated an abundance of small MoS_2 crystals dispersed on the conductive reduced graphene oxide (Figure 6c). Compared with MoS_2 nanoparticles alone (Figure 6d), the introduction of RGO can significantly elevate the catalytic activity of MoS_2, showing a small onset potential of 0.1 V versus RHE and a low Tafel slope of 41 mV dec^{-1}. This Tafel slope is similar to the value for amorphous MoS*x* film (40 mV dec^{-1}).[31] They attributed this to the rich active edge sites due to the reduced sizes of MoS_2 crystals, as well as the enhanced electronic conductance. With the consideration that RGO and MoS_2/RGO are prone to restacking during the hydrothermal process, a novel ternary composite based on two-dimensional MoS_2 supported on nanosized WC decorated RGO was successfully prepared through a similar solvothermal method (Figure 6e),[82] where nanosized tungsten monocarbide (WC) was introduced as a conductive dispersant to prevent GO and RGO from restacking, and the resulting catalyst exhibited excellent HER catalytic performance (Figure 6f).[83] The presence of the conductive and electrocatalytically active nano-WC cloud not only improves the dispersion of MoS_2 but also generates a positive synergistic effect between nano-WC/RGO and layered MoS_2 with respect to the conductivity and porosity. This is a valuable attempt toward the development of advanced MoS_2 nanocatalysts for the HER.

To circumvent conductivity limitations in MoS_2, Jaramillo et al. reported the growth of a core–shell MoO_3/MoS_2 nanowire catalysts by a low-temperature sulfidization method.[30] The resulting hybrids could take advantage of the favorable property of each material, where the substoichiometric MoO_3 serves as a conductive core and the conformal MoS_2 shell serves as both a HER catalyst and a protective layer. This interesting HER catalyst was found to exhibit remarkable current densities (>10 mA/cm^2) at a low overpotential, although it was still limited compared with the MoS_2/RGO. The transmission electron microscopy (TEM) images of the MoO_3/MoS_2 nanowire revealed that most of the MoS_2 basal planes were parallel to the nanowire axis, leading to few edge sites exposed at the surface

dx.doi.org/10.1021/cs500070x | ACS Catal. 2014, 4, 1693−1705

of the nanowires, thus limiting the HER activity on this high-surface-area structure.

Nevertheless, owing to the high surface energy and interlayer van der Waals attractions, 2D nanostructured MoS*x* electrode materials tend to restack or aggregate during the synthesis process or practical applications, which can greatly decrease the performances toward the HER. To further improve the electrocatalytic HER efficiency, the research into three-dimensional (3D) electrode structures for HER has emerged recently.[84] Liu's group used mesoporous graphene foam (MGF) with nanometer scale pores as the matrix to load MoS_2 via an in situ hydrothermal route (Figure 7a).[85] There, the 3D-MGF showed high specific surface area, which in turn provided more space for the growth of the MoS_2 nanoparticles, and thereby increasing exposed active edge sites. Besides, the excellent electrical coupling to the underlying MGF-modified electrode increase the conductivity of the MoS_2 catalyst. Therefore, the obtained MoS_2/MGF nanocomposite demonstrated highly catalytic efficiency for electrochemical hydrogen evolution with a low onset potential of 0.1 V versus RHE and a small Tafel slope of 42 mV dec^{-1} (Figure 7b). Li's group further realized the formation of MoS*x* ($x \geq 2$) catalytic materials on graphene-protected Ni foam with a rigid 3D architecture (Figure 7c,d).[46] The sample obtained at 120 °C showed a current density as high as 44 mA/cm^2 (at −0.2 V vs RHE) (Figure 7e). This excellent catalytic performance of MoS*x*/graphene/3D Ni foam was mainly attributed to the presence of those catalytic species of the bridging S_2^{2-} or apical S^{2-} as well as the increased catalyst loading and conductivity with the use of a 3D graphene/Ni foam support. Followed this work, they presented a similar thermolysis process to produce MoS*x* catalysts on porous 3D sponges.[86] Compared with the MoS*x* grown on 3D graphene-protected Ni foams, a superior HER current density of 71 mA/cm^2 (at −0.2 V vs RHE) was observed for this 3D architecture due to its much higher surface area.

Molecular MoS_2 Edge-Site Mimic. Besides Pt group metals, hydrogenases and nitrogenases are also effective catalysts for the hydrogen evolution process in nature. The active center of these enzymes contains one or more metal atoms (Fe, Ni, or Mo) usually bound to sulfur. When fixating ammonia, these enzyme centers coevolve hydrogen.[11,15] Compared with the individual enzyme molecule, biomimetic electrocatalysts based on chemically synthesized low-cost and earth-abundant metal-containing groups, which resemble the active core groups in redox metalloenzymes, may be able to retain electrocatalytic activity at a small size. The most important advantage of the biomimetic study in the enzyme activity is that it only focuses on the enzymatic center, thereby decreasing the size of electrolysis−catalytic units. From this point, the biomimetic study may offer a particular perspective for the potential use of a molecule/atomic cluster in heterogeneous catalysis and interfacial electrocatalysts. Although in comparison to the MoS*x* nanoparticles, electrocatalysts based on the molecular MoS_2 edge-site mimic contain intrinsically tunable edge sulfur atom with a significant fraction of active sites.

Previously, a molecular MoS*x* compound, incomplete cubane-type $[Mo_3S_4]^{4+}$ clusters, was reported to possess similar sites to nanocrystalline MoS_2 (Figure 8a).[87] This $[Mo_3S_4]^{4+}$-type complex was obtained by reduction of either $(NH_4)_2[MoS_4]$ or $[Mo_2O_2S_2(H_2O)_6]^{2+}$. The obtained $[Mo_3S_4]^{4+}$ complexes contain undercoordinated sulfur to

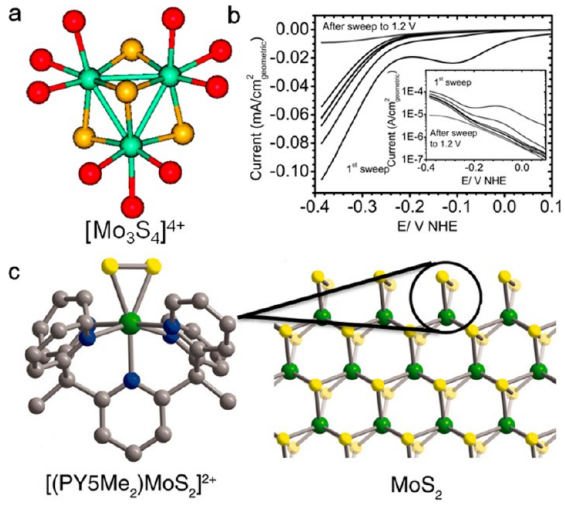

Figure 8. (a) Molecular structure of $[Mo_3S_4]^{4+}$. Blue (Mo), yellow (S), and red (O from water ligands). (b) Polarization curve of the submonolayer of $[Mo_3S_4]^{4+}$ on HOPG in the cathodic region showing hydrogen evolution. Inset: the corresponding Tafel plot. The scan rate was 5 mV/s. (c) $[(PY_5Me_2)MoS_2]^{2+}$ compound designed to mimic the edges of MoS_2. Green (Mo), yellow (S), light blue (F), red (O), blue (N), and gray (C). H atoms are omitted for clarity. Figures reproduced with permission from (a,b) ref 87, Copyright 2008 American Chemical Society; (c) ref 90, Copyright 2012 American Association for the Advancement of Science.

provide active sites for the HER, which were then immobilized on a Toray graphite paper disk or highly oriented pyrolytic graphite (HOPG) for the HER test. At a loading of 0.016 nanomole clusters, 3 orders of magnitude less than that investigated for MoS_2 on fibrous carbon electrodes, these molecular catalysts yielded an onset potential of −0.2 V versus RHE and a Tafel slope of 120 mV dec^{-1} (Figure 8b).[32] This high Tafel slope could be due to diffusion limitations on the planar substrate in a similar manner as was observed for MoS_2 on carbon electrodes.[32] The TOF per $[Mo_3S_4]^{4+}$ cation was found to be 0.07 s^{-1} at $\eta = 0$ mV vs RHE, which is on the same order of magnitude as the TOF of nanoparticulate MoS_2 (0.02 s^{-1}).[16] Unfortunately, the hydrophilicity of the cubane structures could cause an easy peeling off of the catalysts from the electrode surface. These cubanes were also investigated on Au (111), and the same general trends were observed irrespective of substrate.[88]

In addition, Chang et al. identified a Mo^{IV}−oxo complex $[(PY_5Me_2)MoO]^{2+}$ and its ability to catalyze the production of hydrogen from neutral water.[89] Along these lines, they group recently reported a well-defined Mo^{IV}−disulfide molecular $[(PY_5Me_2)MoS_2]^{2+}$, which mimics the structure of the proposed triangular MoS_2 active edge sites, as shown in Figure 8c.[90] The obtained molybdenum−disulfide complex exhibits considerably higher stability and much larger TOFs compared to carbon-supported $[Mo_3S_4]^{4+}$ clusters (~0.07 s^{-1}),[87] and these complexes even showed comparable TOFs to hydrogenase enzymes (which show rates from 10^2 to 10^4 s^{-1}).[91,92] It was expected that the HER properties may be further changed by adjusting the electronic structure of these biomimetic MoS_2 units through ligand modifications. This means that the inherent activity of the catalysts as well as catalyst size would be controllable during the synthesis process. Nevertheless, because those molecular complexes usually suffer loss due to hydrolysis/pyrolysis under extended catalytic condition, the use

dx.doi.org/10.1021/cs500070x | ACS Catal. 2014, 4, 1693−1705

of molecular catalysts always requires more intensive efforts on the design and synthesis of ligands. To overcome those obstacles, Kibsgaard et al. recently reported a similar Mo−S molecular HER catalyst,[93] supported submonolayers of thiomolybdate $[Mo_3S_{13}]^{2-}$ nanoclusters, which exhibited extremely high activity and excellent stability in acid. Significantly, those $[Mo_3S_{13}]^{2-}$ nanoclusters showed the highest HER TOF among any Mo−S catalyst ever synthesized by scalable wet-chemistry methods, which was attributed to the inherently exposed large number of active edge sites by these small $[Mo_3S_{13}]^{2-}$ nanoclusters. Interestingly, in another biomimetic study, H_2 evolution was effectively catalyzed on a liquid water/oil interface (to simulate a cell membrane) by MoS_2, especially, by the mesoporous carbon-supported MoS_2 nanoparticles.[54] When this system was chemically or electrochemically biased by organic electron donors, a remarkable HER activity was observed, effectively demonstrating the versatility of MoS_2 in catalyzing the HER.

CONCLUSION AND OUTLOOK

We summarize the recent progress in the development of MoS*x* nanomaterials as electrocatalysts for the HER. To date, MoS*x* electrodes consisting of various nanostructures (including nanoparticles, nanosheets, films, and composites) have exhibited excellent HER efficiencies, which offer a suitable alternative to the expensive and scarce Pt. It is demonstrated that enhancing the active sites, the conductivity, as well as the inherent activity of different MoS*x* nanostructures are the common strategies in designing effective electrocatalysts for HER. However, many challenges associated with the use of these materials still remain. First, the catalytic activity is greatly affected by the morphology, structure, and density of active sites, and therefore, close attention should be paid to the specific surface area and the composition of the designed MoS*x* nanocatalysts. In this sense, those MoS*x* catalytic materials consisting of small nanoparticles have shown great advantages due to their large amount of active sites, but they are easy to aggregate and show poor stability. The strategy to form porous electrodes may be a feasible way to solve this problem. In the case of ultrathin MoS_2 nanosheets with rich defects, it shows great promises for scalable application, but further optimization of the conductivity remains to be undertaken,[60] whereas the recent attempt to fabricate conductive 1T MoS_2 nanosheets holds immense promise for designing more active MoS_2 catalysts. As for the MoS*x* composite, the choice and design of more conductive and inexpensive substrates with potential synergistic effects is highly desirable.

In addition, the improvement of the inherent activity of MoS*x* catalysts is equally important. Potential strategies include element doping of the MoS*x* host materials, and substrate effects stem from the interaction of substrate with the host catalyst.[72] Although the doping method has not been realized for the active Mo-edge, Co-doping the S-edges to be as active as the Mo-edges is a good example showing how such an effect could be realized. However, doping studies of the Mo-edge of MoS*x* still need further investigation to provide clear insight for the enhanced performance. Specially, the study of the biomimetic and molecular catalysts has presented an alternative strategy using discrete molecular units as catalysts for the HER. Further study could focus on stabilizing the molecular catalysts with suitable substrates, such as the employing of the metal−organic framework (MOF) and exploring other bimetallic organometallic complexes with terminal sulfur ligands synthesized from Mo, Co, W complexes.[10]

Owing to the demand for renewable hydrogen production, the field of the electrochemical HER using MoS*x* has been experiencing a renaissance in recent years. Despite encouraging results in a lab scale, few experiments have demonstrated the use of these catalysts in large-scale applications. Thus, a great deal of effort is still needed to explore the practical use of the efficient advanced electrocatalysts.

AUTHOR INFORMATION

Corresponding Author

*E-mail: WangXin@ntu.edu.sg. Fax: +65 67947553.

Notes

The authors declare no competing financial interest.

ACKNOWLEDGMENTS

Financial support from the academic research fund AcRF tier 1 (M4011020 RG8/12) Ministry of Education, Singapore, and competitive research program (2009 NRF-CRP 001-032), National Research Foundation, Singapore. The support by the Singapore National Research Foundation under its Campus for Research Excellence and Technological Enterprise (CREATE) programme is also acknowledged.

REFERENCES

(1) Balat, M.; Balat, H. *Energy Sources, Part A* **2009**, *31*, 1280.
(2) Turner, J. A. *Science* **2004**, *305*, 972.
(3) Armor, J. N. *Catal. Lett.* **2005**, *101*, 131.
(4) Lasia, A. In *Handbook of Fuel Cells*; John Wiley & Sons, Ltd: Chicester, U.K., 2010; 416.
(5) Phuruangrat, A.; Ham, D. J.; Thongtem, S.; Lee, J. S. *Electrochem. Commun.* **2009**, *11*, 1740.
(6) Kotrel, S.; Bräuninger, S. In *Handbook of Heterogeneous Catalysis*; Wiley-VCH Verlag GmbH & Co. KGaA: Weinheim, 2008; 1936
(7) Tributsch, H.; Bennett, J. C. *J. Electroanal. Chem.* **1977**, *81*, 97.
(8) Jaegermann, W.; Tributsch, H. *Prog. Surf. Sci.* **1988**, *29*, 1.
(9) Gao, M.-R.; Xu, Y.-F.; Jiang, J.; Yu, S.-H. *Chem. Soc. Rev.* **2013**, *42*, 2986.
(10) Chhowalla, M.; Shin, H. S.; Eda, G.; Li, L.-J.; Loh, K. P.; Zhang, H. *Nat. Chem.* **2013**, *5*, 263.
(11) Laursen, A. B.; Kegnaes, S.; Dahl, S.; Chorkendorff, I. *Energy Environ. Sci.* **2012**, *5*, 5577.
(12) Merki, D.; Hu, X. *Energy Environ. Sci.* **2011**, *4*, 3878.
(13) Wang, T.; Gao, D.; Zhuo, J.; Zhu, Z.; Papakonstantinou, P.; Li, Y.; Li, M. *Chem.—Eur. J.* **2013**, *19*, 11939.
(14) Lu, Z.; Zhu, W.; Yu, X.; Zhang, H.; Li, Y.; Sun, X.; Wang, X.; Wang, H.; Wang, J.; Luo, J.; Lei, X.; Jiang, L. *Adv. Mater.* **2014**, DOI: 10.1002/adma.201304759.
(15) Hinnemann, B.; Moses, P. G.; Bonde, J.; Jørgensen, K. P.; Nielsen, J. H.; Horch, S.; Chorkendorff, I.; Nørskov, J. K. *J. Am. Chem. Soc.* **2005**, *127*, 5308.
(16) Jaramillo, T. F.; Jørgensen, K. P.; Bonde, J.; Nielsen, J. H.; Horch, S.; Chorkendorff, I. *Science* **2007**, *317*, 100.
(17) Liu, R.; Duay, J.; Lee, S. B. *Chem. Commun.* **2011**, *47*, 1384.
(18) MyriamPerezdela, R.; Russell, R. C. In *Dekker Encyclopedia of Nanoscience and Nanotechnology*, 2nd ed.; CRC Press: Boca Raton, Florida, 2008; p 3080.
(19) Chang, K.; Chen, W. *ACS Nano* **2011**, *5*, 4720.
(20) Rapoport, L.; Moshkovich, A.; Perfilyev, V.; Laikhtman, A.; Lapsker, I.; Yadgarov, L.; Rosentsveig, R.; Tenne, R. *Tribol. Lett.* **2012**, *45*, 257.
(21) Xiang, Q.; Yu, J.; Jaroniec, M. *J. Am. Chem. Soc.* **2012**, *134*, 6575.
(22) Zong, X.; Wu, G.; Yan, H.; Ma, G.; Shi, J.; Wen, F.; Wang, L.; Li, C. *J. Phys. Chem. C* **2010**, *114*, 1963.

(23) Zhao, Y.; Zhang, Y.; Yang, Z.; Yan, Y.; Sun, K. *Sci. Technol. Adv. Mater.* **2013**, *14*, 043501.
(24) Yang, J.; Shin, H. S. *J. Mater. Chem. A* **2014**, DOI: 10.1039/c3ta14151a.
(25) Trasatti, S. *J. Electroanal. Chem.* **1972**, *39*, 163.
(26) Conway, B. E.; Angerstein, x; Kozlowska, H.; Ho, F. C. *J. Vac. Sci. Technol.* **1977**, *14*, 351.
(27) Conway, B. E.; Tilak, B. V. *Electrochim. Acta* **2002**, *47*, 3571.
(28) Kibsgaard, J.; Chen, Z.; Reinecke, B. N.; Jaramillo, T. F. *Nat. Mater.* **2012**, *11*, 963.
(29) Li, Y.; Wang, H.; Xie, L.; Liang, Y.; Hong, G.; Dai, H. *J. Am. Chem. Soc.* **2011**, *133*, 7296.
(30) Chen, Z.; Cummins, D.; Reinecke, B. N.; Clark, E.; Sunkara, M. K.; Jaramillo, T. F. *Nano Lett.* **2011**, *11*, 4168.
(31) Merki, D.; Fierro, S.; Vrubel, H.; Hu, X. L. *Chem. Sci.* **2011**, *2*, 1262.
(32) Bonde, J.; Moses, P. G.; Jaramillo, T. F.; Norskov, J. K.; Chorkendorff, I. *Faraday Discuss.* **2009**, *140*, 219.
(33) Albu-Yaron, A.; Levy, M.; Tenne, R.; Popovitz-Biro, R.; Weidenbach, M.; Bar-Sadan, M.; Houben, L.; Enyashin, A. N.; Seifert, G.; Feuermann, D.; Katz, E. A.; Gordon, J. M. *Angew. Chem., Int. Ed.* **2011**, *50*, 1810.
(34) Lauritsen, J. V.; Kibsgaard, J.; Helveg, S.; Topsoe, H.; Clausen, B. S.; Laegsgaard, E.; Besenbacher, F. *Nat. Nanotechnol.* **2007**, *2*, 53.
(35) McDonnell, S.; Addou, R.; Buie, C.; Wallace, R. M.; Hinkle, C. L. *ACS Nano* **2014**, DOI: 10.1021/nn500044q.
(36) Conway, B. E.; Bai, L.; Sattar, M. A. *Int. J. Hydrogen Energy* **1987**, *12*, 607.
(37) Boudart, M. *Chem. Rev.* **1995**, *95*, 661.
(38) Late, D. J.; Liu, B.; Matte, H. S. S. R.; Dravid, V. P.; Rao, C. N. R. *ACS Nano* **2012**, *6*, 5635.
(39) Kisielowski, C.; Ramasse, Q. M.; Hansen, L. P.; Brorson, M.; Carlsson, A.; Molenbroek, A. M.; Topsøe, H.; Helveg, S. *Angew. Chem., Int. Ed.* **2010**, *49*, 2708.
(40) Huang, X.; Zeng, Z.; Zhang, H. *Chem. Soc. Rev.* **2013**, *42*, 1934.
(41) Tran, P. D.; Wong, L. H.; Barber, J.; Loo, J. S. C. *Energy Environ. Sci.* **2012**, *5*, 5902.
(42) Helveg, S.; Lauritsen, J. V.; Lægsgaard, E.; Stensgaard, I.; Nørskov, J. K.; Clausen, B. S.; Topsøe, H.; Besenbacher, F. *Phys. Rev. Lett.* **2000**, *84*, 951.
(43) Lauritsen, J. V.; Bollinger, M. V.; Lægsgaard, E.; Jacobsen, K. W.; Nørskov, J. K.; Clausen, B. S.; Topsøe, H.; Besenbacher, F. *J. Catal.* **2004**, *221*, 510.
(44) Hinnemann, B.; Nørskov, J. K.; Topsøe, H. *J. Phys. Chem. B* **2004**, *109*, 2245.
(45) Brorson, M.; Carlsson, A.; Topsøe, H. *Catal. Today* **2007**, *123*, 31.
(46) Chang, Y.-H.; Lin, C.-T.; Chen, T.-Y.; Hsu, C.-L.; Lee, Y.-H.; Zhang, W.; Wei, K.-H.; Li, L.-J. *Adv. Mater.* **2013**, *25*, 756.
(47) Kong, D.; Wang, H.; Cha, J. J.; Pasta, M.; Koski, K. J.; Yao, J.; Cui, Y. *Nano Lett.* **2013**, *13*, 1341.
(48) Vrubel, H.; Merki, D.; Hu, X. *Energy Environ. Sci.* **2012**, *5*, 6136.
(49) Benck, J. D.; Chen, Z.; Kuritzky, L. Y.; Forman, A. J.; Jaramillo, T. F. *ACS Catal.* **2012**, *2*, 1916.
(50) Ge, X.; Chen, L.; Zhang, L.; Wen, Y.; Hirata, A.; Chen, M. *Adv. Mater.* **2014**, DOI: 10.1002/adma.201305678.
(51) Tsai, C.; Abild-Pedersen, F.; Nørskov, J. K. *Nano Lett.* **2014**, *14*, 1381.
(52) Najmaei, S.; Zou, X.; Er, D.; Li, J.; Jin, Z.; Gao, W.; Zhang, Q.; Park, S.; Ge, L.; Lei, S.; Kono, J.; Shenoy, V. B.; Yakobson, B. I.; George, A.; Ajayan, P. M.; Lou, J. *Nano Lett.* **2014**, *14*, 1354.
(53) Vrubel, H.; Moehl, T.; Gratzel, M.; Hu, X. *Chem. Commun.* **2013**, *49*, 8985.
(54) Ge, P.; Scanlon, M. D.; Peljo, P.; Bian, X.; Vubrel, H.; O'Neill, A.; Coleman, J. N.; Cantoni, M.; Hu, X.; Kontturi, K.; Liu, B.; Girault, H. H. *Chem. Commun.* **2012**, *48*, 6484.
(55) Huang, X.; Zeng, Z.; Bao, S.; Wang, M.; Qi, X.; Fan, Z.; Zhang, H. *Nat. Commun.* **2013**, *4*, 1444.
(56) Kim, J.; Byun, S.; Smith, A. J.; Yu, J.; Huang, J. *J. Phys. Chem. Lett.* **2013**, *4*, 1227.
(57) Yu, Y.; Huang, S.-Y.; Li, Y.; Steinmann, S. N.; Yang, W.; Cao, L. *Nano Lett.* **2014**, *14*, 553.
(58) Yan, Y.; Xia, B. Y.; Ge, X.; Liu, Z.; Wang, J.-Y.; Wang, X. *ACS Appl. Mater. Interfaces* **2013**, *5*, 12794.
(59) Xie, J.; Zhang, H.; Li, S.; Wang, R.; Sun, X.; Zhou, M.; Zhou, J.; Lou, X. W.; Xie, Y. *Adv. Mater.* **2013**, *25*, 5807.
(60) Xie, J.; Zhang, J.; Li, S.; Grote, F.; Zhang, X.; Zhang, H.; Wang, R.; Lei, Y.; Pan, B.; Xie, Y. *J. Am. Chem. Soc.* **2013**, *136*, 1680.
(61) Spirko, J. A.; Neiman, M. L.; Oelker, A. M.; Klier, K. *Surf. Sci.* **2003**, *542*, 192.
(62) Lau, V. W.-h.; Masters, A. F.; Bond, A. M.; Maschmeyer, T. *ChemCatChem.* **2011**, *3*, 1739.
(63) Lau, V. W.-h.; Masters, A. F.; Bond, A. M.; Maschmeyer, T. *Chem.—Eur. J.* **2012**, *18*, 8230.
(64) Jiménez Sandoval, S.; Yang, D.; Frindt, R. F.; Irwin, J. C. *Phys. Rev. B* **1991**, *44*, 3955.
(65) Wypych, F.; Schollhorn, R. *Chem. Commun.* **1992**, 1386.
(66) Lukowski, M. A.; Daniel, A. S.; Meng, F.; Forticaux, A.; Li, L.; Jin, S. *J. Am. Chem. Soc.* **2013**, *135*, 10274.
(67) Voiry, D.; Salehi, M.; Silva, R.; Fujita, T.; Chen, M.; Asefa, T.; Shenoy, V. B.; Eda, G.; Chhowalla, M. *Nano Lett.* **2013**, *13*, 6222.
(68) Murugesan, S.; Akkineni, A.; Chou, B. P.; Glaz, M. S.; Vanden Bout, D. A.; Stevenson, K. J. *ACS Nano* **2013**, *7*, 8199.
(69) Tran, P. D.; Pramana, S. S.; Kale, V. S.; Nguyen, M.; Chiam, S. Y.; Batabyal, S. K.; Wong, L. H.; Barber, J.; Loo, J. *Chem.—Eur. J.* **2012**, *18*, 13994.
(70) Bandarenka, A. S.; Varela, A. S.; Karamad, M.; Calle-Vallejo, F.; Bech, L.; Perez-Alonso, F. J.; Rossmeisl, J.; Stephens, I. E. L.; Chorkendorff, I. *Angew. Chem., Int. Ed.* **2012**, *51*, 11845.
(71) Morales-Guio, C. G.; Tilley, S. D.; Vrubel, H.; Grätzel, M.; Hu, X. *Nat. Commun.* **2014**, *5*, 3059.
(72) Wang, T.; Liu, L.; Zhu, Z.; Papakonstantinou, P.; Hu, J.; Liu, H.; Li, M. *Energy Environ. Sci.* **2013**, *6*, 625.
(73) Merki, D.; Vrubel, H.; Rovelli, L.; Fierro, S.; Hu, X. *Chem. Sci.* **2012**, *3*, 2515.
(74) Tran, P. D.; Nguyen, M.; Pramana, S. S.; Bhattacharjee, A.; Chiam, S. Y.; Fize, J.; Field, M. J.; Artero, V.; Wong, L. H.; Loo, J.; Barber, J. *Energy Environ. Sci.* **2012**, *5*, 8912.
(75) Tran, P. D.; Chiam, S. Y.; Boix, P. P.; Ren, Y.; Pramana, S. S.; Fize, J.; Artero, V.; Barber, J. *Energy Environ. Sci.* **2013**, *6*, 2452.
(76) Yadgarov, L.; Rosentsveig, R.; Leitus, G.; Albu-Yaron, A.; Moshkovich, A.; Perfilyev, V.; Vasic, R.; Frenkel, A. I.; Enyashin, A. N.; Seifert, G.; Rapoport, L.; Tenne, R. *Angew. Chem., Int. Ed.* **2012**, *51*, 1148.
(77) Wang, H.; Kong, D.; Johanes, P.; Cha, J. J.; Zheng, G.; Yan, K.; Liu, N.; Cui, Y. *Nano Lett.* **2013**, *13*, 3426.
(78) Yan, Y.; Ge, X.; Liu, Z.; Wang, J.-Y.; Lee, J.-M.; Wang, X. *Nanoscale* **2013**, *5*, 7768.
(79) Lin, T.-W.; Liu, C.-J.; Lin, J.-Y. *Appl. Catal., B* **2013**, *134*−*135*, 75.
(80) Bian, X.; Zhu, J.; Liao, L.; Scanlon, M. D.; Ge, P.; Ji, C.; Girault, H. H.; Liu, B. *Electrochem. Commun.* **2012**, *22*, 128.
(81) Li, D. J.; Maiti, U. N.; Lim, J.; Choi, D. S.; Lee, W. J.; Oh, Y.; Lee, G. Y.; Kim, S. O. *Nano Lett.* **2014**, *14*, 1228.
(82) Yan, Y.; Xia, B.; Qi, X.; Wang, H.; Xu, R.; Wang, J.-Y.; Zhang, H.; Wang, X. *Chem. Commun.* **2013**, *49*, 4884.
(83) Bennett, L. H.; Cuthill, J. R.; McAlister, A. J.; Erickson, N. E.; Watson, R. E. *Science* **1974**, *184*, 563.
(84) Wang, P.-p.; Sun, H.; Ji, Y.; Li, W.; Wang, X. *Adv. Mater.* **2014**, *26*, 964.
(85) Liao, L.; Zhu, J.; Bian, X.; Zhu, L.; Scanlon, M. D.; Girault, H. H.; Liu, B. *Adv. Funct. Mater.* **2013**, *23*, 5326.
(86) Chang, Y.-H.; Wu, F.-Y.; Chen, T.-Y.; Hsu, C.-L.; Chen, C.-H.; Wiryo, F.; Wei, K.-H.; Chiang, C.-Y.; Li, L.-J. *Small* **2014**, *10*, 895.
(87) Jaramillo, T. F.; Bonde, J.; Zhang, J.; Ooi, B.-L.; Andersson, K.; Ulstrup, J.; Chorkendorff, I. *J. Phys. Chem. C* **2008**, *112*, 17492.

(88) Kristensen, J.; Zhang, J.; Chorkendorff, I.; Ulstrup, J.; Ooi, B. L. *Dalton Trans.* **2006**, 3985.
(89) Karunadasa, H. I.; Chang, C. J.; Long, J. R. *Nature* **2010**, *464*, 1329.
(90) Karunadasa, H. I.; Montalvo, E.; Sun, Y.; Majda, M.; Long, J. R.; Chang, C. J. *Science* **2012**, *335*, 698.
(91) Frey, M. *ChemBioChem* **2002**, *3*, 153.
(92) Cracknell, J. A.; Vincent, K. A.; Armstrong, F. A. *Chem. Rev.* **2008**, *108*, 2439.
(93) Kibsgaard, J.; Jaramillo, T. F.; Besenbacher, F. *Nat. Chem.* **2014**, *6*, 248.